



## ISTITUTO NAZIONALE DI RICERCA METROLOGICA Repository Istituzionale

Supramolecular topological adhesion boosts delamination resistance in carbon fiber reinforced polymers

*Original*

Supramolecular topological adhesion boosts delamination resistance in carbon fiber reinforced polymers / Milani, M.; D'Auria, S.; Bertocchi, F.; Boschetti, A.; Lapini, A.; Fina, A.; Pedrini, A.; Pinalli, R.; Pernechele, C.; Dalcanale, E.. - In: ADVANCED COMPOSITES AND HYBRID MATERIALS. - ISSN 2522-0136. - 9:1(2025). [10.1007/s42114-025-01569-7]

*Availability:*

This version is available at: 11696/88882 since: 2026-03-02T15:09:08Z

*Publisher:*

Springer Science and Business Media B.V.

*Published*

DOI:10.1007/s42114-025-01569-7

*Terms of use:*

This article is made available under terms and conditions as specified in the corresponding bibliographic description in the repository

*Publisher copyright*

(Article begins on next page)



# Supramolecular topological adhesion boosts delamination resistance in carbon fiber reinforced polymers

Monica Milani<sup>1</sup> · Silvia D'Auria<sup>1</sup> · Francesco Bertocchi<sup>1</sup> · Alice Boschetti<sup>4,5</sup> · Andrea Lapini<sup>1,5</sup> · Alberto Fina<sup>2</sup> · Alessandro Pedrini<sup>1</sup> · Roberta Pinalli<sup>1</sup> · Chiara Pernechele<sup>3</sup> · Enrico Dalcanale<sup>1</sup>

Received: 29 January 2025 / Revised: 9 October 2025 / Accepted: 26 November 2025  
© The Author(s) 2025

## Abstract

In this study, we introduce supramolecular topological adhesion as an innovative and effective methodology to enhance interlaminar fracture toughness in carbon fiber reinforced polymers (CFRPs). We achieved remarkable improvements in delamination resistance by physically entangling phenoxy resins within an epoxy matrix and introducing sacrificial H-bond interactions via ODIN (1-(7-Oxo-7,8-Dihydro-1,8-Naphthyridin-2-yl)urea) units. The ODIN units form sextuple H-bonding dimers in the cured epoxy matrix among plies, experimentally quantified via UV–Vis spectroscopy, whose detachment hinders crack propagation. The viability of this approach was tested using various phenoxy resins with different molecular weights and with different levels of ODIN functionalization. Single lap shear (SLS) tests demonstrated a notable increase in adhesion strength, pointing out PKHB-ODIN 13% as the best candidate as interlaminar adherent. Delamination resistance was determined through double cantilever beam (DCB) and end-notched flexure (ENF) tests, showing up to 120% and 80% increases in Mode I and Mode II fracture toughness, respectively. The limited DCB and ENF test increments observed for control adherent PKHB-PU 23% functionalized with phenylurea (PU) groups, demonstrates that the strength of topological H-bonding is pivotal to boost delamination resistance. The results indicate that this method holds great potential for improving the durability of CFRP composites, especially in applications requiring high resistance to delamination.

**Keywords** Supramolecular topological adhesion · Sextuple H-bonds · Delamination resistance · Carbon fiber reinforced polymers

## 1 Introduction

Laminate composites are multilayer materials where each layer is composed by fibers oriented unidirectionally or stitched in matt structures. Among fiber-reinforced composites, carbon fiber reinforced polymers (CFRPs) have become the material of choice for advanced structural applications requiring superior mechanical performance and reduced weight. Their widespread adoption in aerospace, automotive, wind energy, and high-performance sporting goods is primarily attributed to their high specific strength and stiffness, excellent fatigue resistance, and inherent corrosion resistance [1]. CFRP laminates are commonly fabricated by stacking prepregs—carbon fiber sheets pre-impregnated with thermosetting matrices, typically epoxy resins—to produce tailored, anisotropic structures optimized for specific loading conditions [2].

✉ Enrico Dalcanale  
enrico.dalcanale@unipr.it

<sup>1</sup> Department of Chemistry, Life Sciences and Environmental Sustainability and INSTM UdR Parma, University of Parma, Parco Area Delle Scienze 17/A, 43124 Parma, Italy  
<sup>2</sup> Dipartimento Di Scienza Applicata E Tecnologia, Politecnico Di Torino, Viale Teresa Michel 5, 15121 Alessandria, Italy  
<sup>3</sup> Dallara S.P.A., Via Provinciale 33, 43040 Varano de' Melegari, Italy  
<sup>4</sup> Istituto Nazionale Di Ricerca Metrologica (INRIM), 10135 Turin, Italy  
<sup>5</sup> European Laboratory for Non-Linear Spectroscopy (LENS), Sesto Fiorentino, Italy

Delamination is a predominant failure mode in CFRP laminate materials, characterized by the separation of layers (plies) due to weak interfacial bonding [3]. This loss of cohesion significantly degrades the mechanical properties of the composite, compromising both its load-bearing capacity and service life. Delamination can be initiated by factors such as manufacturing defects, geometric discontinuities (e.g., edges, corners, holes, and notches), and impact damage. It is particularly critical in complex structures like aircraft skin-stringer assemblies and tapered components. Delamination is indeed the most common failure mechanism in laminated composites [4], especially under impact or out-of-plane loading conditions.

Several approaches have been implemented to improve interlaminar fracture toughness in CFRPs: (i) matrix toughening with rubber [5], fibers [6] or nanofillers like carbon nanotubes [7, 8]; (ii) interleaving, placing thermoplastic films or fiber mats at interfaces between neighboring plies [9]; (iii) Z-pinning by inserting pins perpendicular to the laminate plane [10] or stitching fibers [11] through the laminate thickness; (iv) surface treatments of carbon fibers like fiber sizing and plasma treatment [12]; (v) optimized ply stacking sequence [13]; (vi) resin modification with reactive tougheners or hyperbranched polymers [14]. The interleaving approach has been also implemented using H-bonded supramolecular polymers as interleave additives, leading to increased interlaminar fracture toughness and partial self-healing capabilities [15].

Topological adhesion is a potential alternative to these approaches, already employed to enhance interfacial adhesion between hydrogels [16]. In this context, topological adhesion refers to linking two polymer networks, called adherends, through a third polymer, named stitch polymer. The latter diffuses into the two adherends and crosslinks into a third polymer network in situ, in topological entanglement with the adherends networks. As a result, the third polymer network joins the other two networks together like a molecular suture. However, the presence of extensive covalent crosslinking among plies has an adverse effect on the interlaminar toughness. In polymeric materials, the introduction of multiple H-bonding crosslinking can reverse this trend by boosting toughness without sacrificing mechanical strength [17]. In the specific case of CFRP, this effect should lead to an interlaminar fracture toughness increase, since the elastic modulus is governed by the carbon fiber component. Differently, physical entanglement refers to the intertwining or interlocking of polymer chains through physical interactions, without the formation of covalent networks.

Here we report an innovative method to enhance interlaminar fracture toughness in CFRPs based on *supramolecular topological adhesion*. The proposed approach combines the physical entanglement of phenoxy resins

within the CFRP epoxy matrix with sacrificial H-bond interactions among ODIN (acronym for 1-(7-Oxo-7,8-Dihydro-1,8-Naphthyridin-2-yl)urea) units, introduced as lateral substituents in the phenoxy resin. The overall effect of this supramolecular topological entanglement among plies (Fig. 1) is the amplification of interfacial toughness, leading to enhanced delamination resistance.

Phenoxy resins are commercially available amorphous thermoplastic polymers with molecular weight in the range 10,000–100,000 g/mol, miscible with epoxy resins. The pendant secondary hydroxyl groups in phenoxy resins are amenable to a variety of functionalizations. Due to their excellent mechanical properties including flexibility, toughness, adhesive and cohesive strength, as well as chemical and heat resistance, phenoxy resins are widely employed in composites and adhesives [18]. We recently introduced ODIN as sextuple H-bonding array motif, capable of self-dimerizing both in solution and in a polymeric matrix [19]. ODIN features a high self-dimerization constant measured in solution ( $K_{\text{dim}} = 4 \cdot 10^4 \text{ M}^{-1}$ ) and a remarkable thermal stability.<sup>19</sup> Another relevant property of ODIN is the different fluorescence [20] and UV–Vis [21] signature of the monomer and the dimer, allowing to quantify the dimer/monomer ratio in a polymer matrix. To be grafted on polymers ODIN is typically functionalized with an isocyanate group, which is also reactive toward the hydroxyl groups present on the phenoxy resins.

For this study, we selected a CFRP that has wide application in the automotive sector, due to its valuable mechanical properties, in terms of compression strength and for the possibility of being processed at different temperatures.

## 2 Methodology

### 2.1 Material preparation

The material chosen for the present work is a commercial prepreg, realized by CIT Toray company, C384 T700 12 K 2X2T ER450 40% Hot melt. This material is characterized by an aerial weight of dry fiber of 384 g/m<sup>2</sup> and it is realized

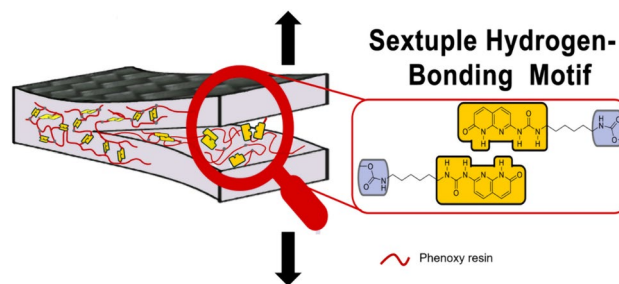


**Fig. 1** Sketch of the proposed supramolecular topological adhesion operation

with a Toray T700 fiber (high strength fiber with fiber tensile modulus  $E=230$  GPa and strength  $\sigma=4.9$  GPa.). The resin is ER-450 and it is a toughened epoxy matrix, that can be cured in a variety of conditions, from  $80$  °C up to  $180$  °C. It is characterized by a maximum glass transition temperature of  $210$  °C. After a cure cycle of 2 h at  $135$  °C it exhibits a  $T_g$  of  $160$  °C. This material is widely used in racing and automotive sectors. It is characterized by high mechanical properties in compression loading, while its interlaminar properties are less pronounced.

## 2.2 Single Lap Shear (SLS) test procedure

*Preparation of tests specimens for lap shear tests according to ASTM D 5868.* Two CFRP panels ( $150 \times 200$  mm) were laminated with 8 plies each and the adhesives were deposited on the surface of one plate in a section of  $200 \text{ mm} \times 30 \text{ mm}$  to cover the overlap length ( $25.4$  mm for the standard used).

The adhesive was dissolved in a mixture of chloroform and hexafluoroisopropanol (ratio 9:1, 2 mL per specimen, 250 mg of adhesive) and added with a brush (Fig. 2a). After waiting 24 h to ensure solvent evaporation, the panel was laminated and cured in autoclave for 90 min  $135$  °C, 6 bars (Fig. 2b,c). After the curing phase, 6 specimens of dimension  $175 \text{ mm} \times 25 \text{ mm} \times 3 \text{ mm}$  were obtained using a robot with waterjet cutting (Fig. 2d).

*Lap shear tests.* Lap shear tests were performed with an electromechanical testing machine MTS Insight 150 kN, with 250 kN hydraulic grips. The position of the transducer LVDT is 300 mm, with a resolution of 0.001 mm. The tensile tester is equipped with a load cell of 150 kN, with a resolution of 0.002 kN class 0.5. The test speed is: 2 mm/min.

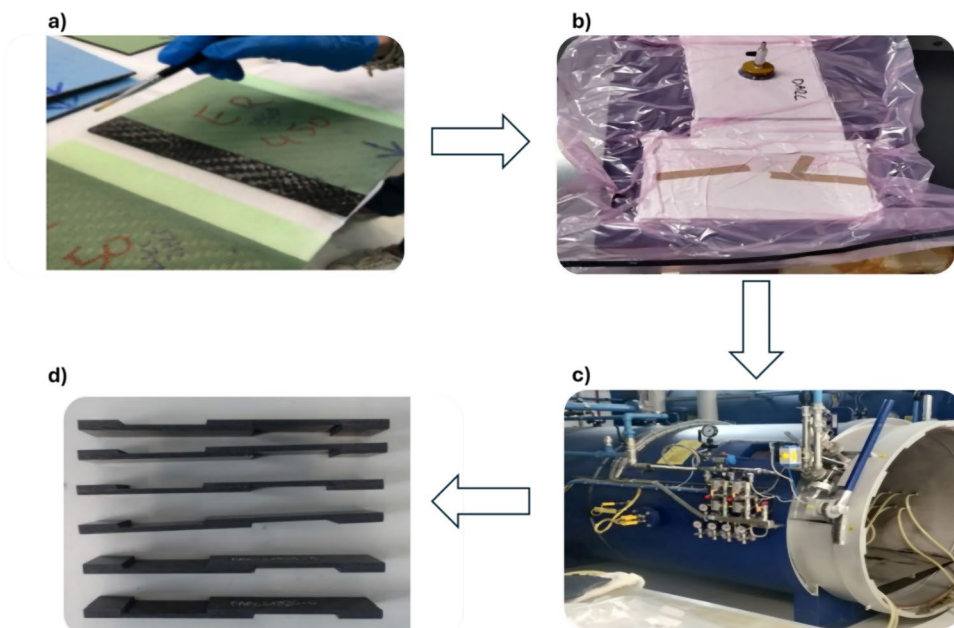
## 2.3 Delamination tests

DCB specimens were prepared similarly to the SLS specimens with the only difference that the panels are totally superimposed (Figure S17A). The specimens have the following final dimensions: 150 mm total length, 25 mm width, 26 mm crack length, and were tested under a 3.0 mm/min crosshead separation rate (Figure S17B). Aluminum blocks were fixed with epoxy resin glue on the tip for the application of the load (Figure S18A). The amount of adhesive applied on the uncured plies on a joint area of  $250 \text{ mm} \times 250 \text{ mm}$  is 2,60 g dissolved in 30 mL of a solution of chloroform and hexafluoroisopropanol 9:1 (Fig. 2a). After 24 h, the samples underwent a vacuum bag phase before being cured in autoclave for 90 min at  $135$  °C and 6 bars of pressure (Fig. 2b, c). The specimens were obtained by cutting out the CFRP panel using a robot equipped with waterjet cutting. DCB and ENF samples were realized from the same panel. This allows us to guarantee the same functionalization and ensure higher reproducibility and conditions consistency.

ENF specimens have the following dimensions: 180 mm total length, 25 mm width, 55 mm crack length, and were tested under a 1.0 mm/min crosshead separation rate. ENF tests were carried out with 100 mm span between supports, and the specimen placed in the 3-point bending geometry as follows: 55 mm specimen half-span and 30 mm delamination length (Figures S17B, S18B and S20).

The energy for unit length  $G_I$  was evaluated considering a crack length range of 48–80 mm for DCB, while for ENF tests, once the cracks propagate the test is concluded. The peak in the force/displacement diagram is considered representative of the above-described event. A further evaluation

**Fig. 2** Process of preparation of lap shear specimens: **a** application of the adhesives on the selected area of the ply, **b** joint panels were placed in a vacuum bag, **c** autoclave used for the curing cycle and **d** lap shear specimens obtained



of the results was also realized considering the initial displacement measured by the Digital Image Correlation (DIC) camera. The experimental set up for both tests are shown in Figures S19 and S20 respectively.

The  $G_I$  that is necessary for creep propagation is calculated with the *Modified Beam Theory (MBT) Method* (ASTM D5528-13) according to Eq. (1):

$$G_I = \frac{3P\delta}{2B(\alpha + |\Delta|)} \left[ \frac{N}{mm} \right] \quad (1)$$

where  $P$  is the applied load,  $\delta$  is the displacement,  $B$  is the specimen width,  $a$  refers to the crack length and  $\Delta$  is an empirical constant. A ZEISS ARAMIS 3D Camera was used to monitor the crack propagation (Figure S19 right).

Similarly, in ENF tests,  $G_{II}$  is calculated following the standard D7905/D7905M considering  $P$  as the applied load,  $B$  is the specimen width,  $a$  is the crack length and  $m$  is the compliance constant, corresponding to the slope of the regression curve calculated with the compliance calibration test, according to Eq. (2):

$$G_{II} = \frac{P^2}{2b} \cdot \frac{dC}{da} = \frac{3mP^2a^2}{2B} \left[ \frac{N}{mm} \right] \quad (2)$$

The compliance calibration test is performed measuring the compliance of the specimen at 20 cm and 40 cm from the initial crack length. The displacement of the two adherend is monitored with ZEISS ARAMIS 3D Camera.

### 3 Results and discussion

#### 3.1 Synthesis of the model compound 1

A model reaction between ODIN isocyanate and isopropanol was performed with the aim of setting the best reaction conditions for ODIN grafting on phenoxy resins (Scheme S2). Isopropanol was chosen as the simplest reagent to mimic the reactivity of the secondary alcohols of the phenoxy resins. The reaction was performed in DMSO to dissolve ODIN-isocyanate (Scheme S1), using a large excess of isopropanol to mimic the large number of secondary OHs of the phenoxy resins. DABCO (1,4-diazabicyclo[2.2.2]octane) was added to catalyze the reaction that was kept at 70 °C overnight. The reaction mixture was then cooled at room temperature and the final product was obtained in quantitative yield by precipitation with water, followed by repeated washing of the precipitate with water to remove traces of DMSO and DABCO. ODIN dimerization is suppressed in good hydrogen-bond acceptor solvents like DMSO.<sup>19</sup> ODIN shows two main tautomeric conformers when dissolved in DMSO- $d_6$ ,

as reported by Loos and coworkers [19, 22]. The keto conformer **1a** is the dominant one, forming a six-membered ring with intramolecular N–H⋯N H-bonding in accordance with Etter's rule [23] (Figure S2 and Fig. 3, blue dots). This monomer is formed by first breaking the intermolecular hydrogen bond of the ODIN dimer and the  $\pi$ - $\pi$  stacking and the weak intermolecular C–H⋯O=C hydrogen bond that permits the rotation to form a stronger N–H⋯N bond. The second observed conformer **1b** in DMSO- $d_6$  is the keto monomer without intramolecular H-bonding (Figure S2 and Fig. 3, orange dots).

#### 3.2 General procedure for the functionalization of phenoxy resin PKHB with ODIN and PU

Three different grades of commercial phenoxy resins having increasing  $M_w$  were selected: PKHA ( $M_w=25000$ ), PKHB ( $M_w=32000$ ) and PKHP ( $M_w=52000$ ). As shown in the lap-shear test section, PKHB is the best performing resin in terms of physical entanglement, therefore we focused on PKHB as polymer matrix for ODIN functionalization. To distinguish the influence of ODIN dimerization from the traditional hydrogen bonding network, PKHB was also functionalized using phenylureidohexyl isocyanate (PU). The corresponding PKHB-PU polymer features phenylurea dangling groups capable of standard H-bonding in the matrix.

Reaction of ODIN-isocyanate with PKHB using the conditions applied for the synthesis of **1** lead to the partial functionalization of the secondary OH groups of the polymer (Scheme 1). Methyl ethyl ketone (MEK) is added as cosolvent to increase PKHB solubility. Two different grades of PKHB-ODIN are obtained by varying the amount of ODIN-isocyanate added: PKHB-ODIN 8% and PKHB-ODIN 13%. The degree of functionalization of the two polymers was experimentally determined by elemental analysis since nitrogen is introduced exclusively with the ODIN units (Table S1). The formation of the urethane bond leads to the appearance of a broad triplet at 7.34 ppm, (F signal, Fig. 3 and Figure S3) corresponding to the N–H signal of the urethane and a multiplet for the methine group of functionalized phenoxy resin at 5.19 ppm (I signal, Fig. 3). The unreacted OH signal of PKHB is visible as doublet at 5.34 ppm (M signal, Fig. 3), while the methyne groups of the unreacted phenoxy resin resonate at 4.1 ppm (L signal, Fig. 3). The ATR FTIR spectrum of PHKB-ODIN samples shows a peak at 1710  $\text{cm}^{-1}$  related to the stretching of the carbamate carbonyl (Figure S4). In solution, the polymer grafted ODIN assumes the same two conformations already observed in model compound **1**, as shown by the blue and orange <sup>1</sup>H NMR signal attribution in Fig. 3. The relative ratio of the two ODIN conformers grafted to the polymer is 7:1 in favor of the blue conformer.

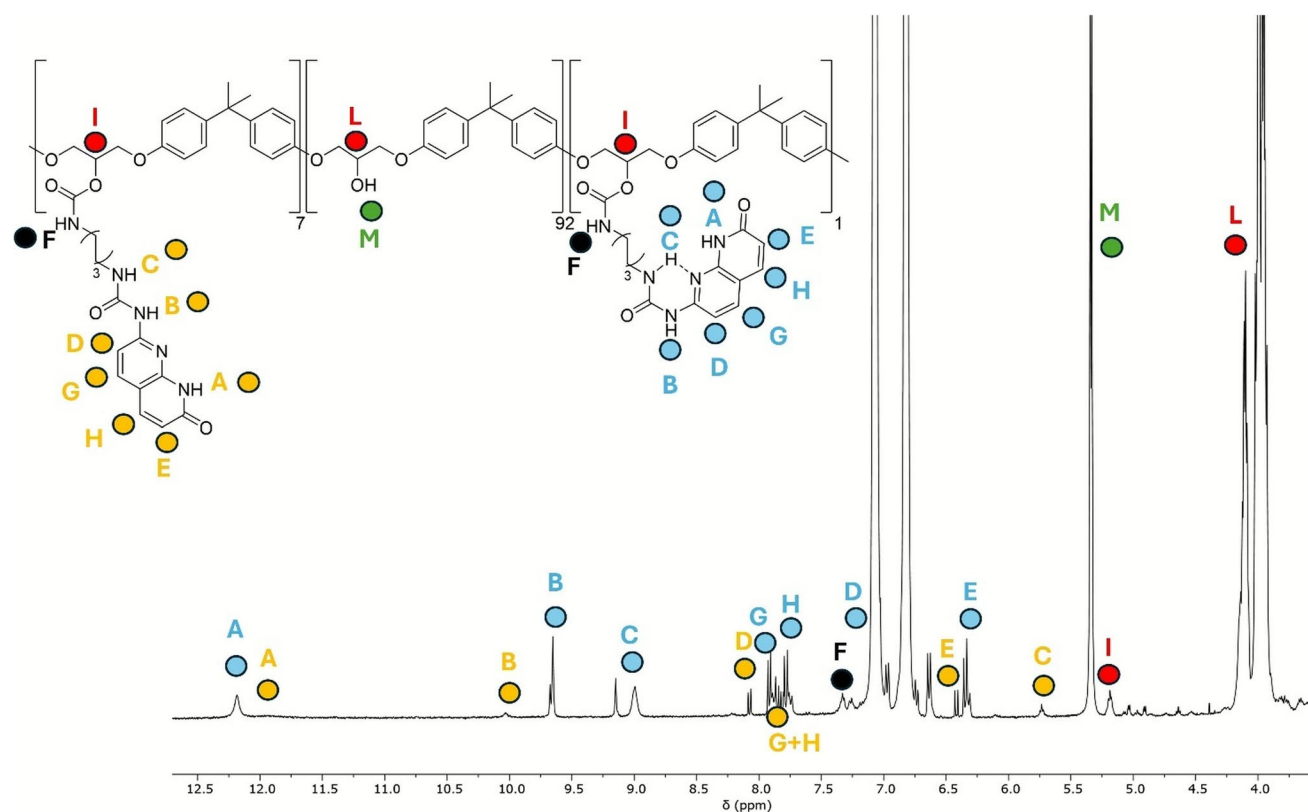


**Fig. 3** Selected portion of the  $^1\text{H}$  NMR ( $\text{DMSO-}d_6$ , 298 K, 600 MHz) of PKHB-ODIN 8%

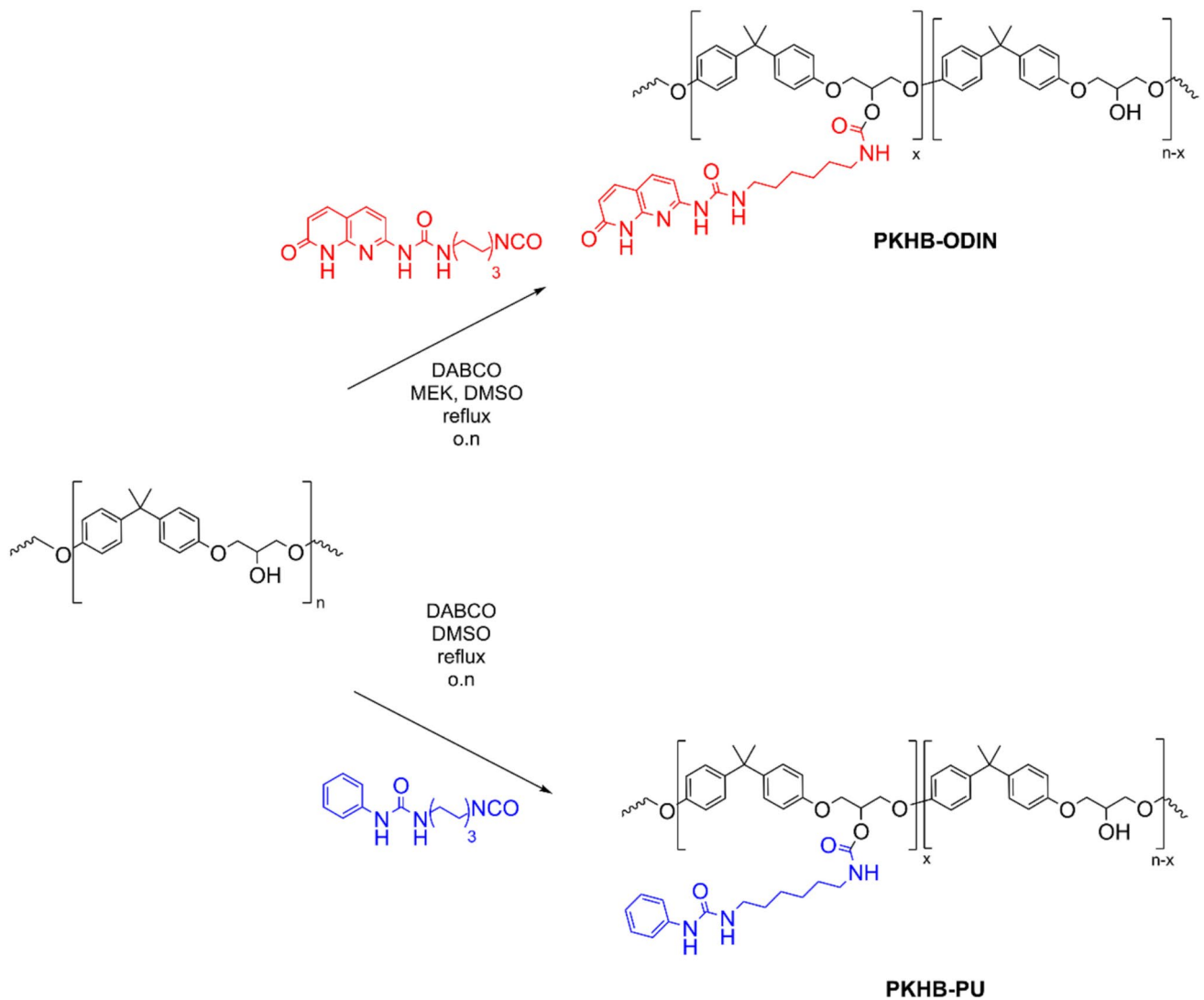
For a proper comparison of the effect of ODIN multiple H-bonding dimerization pattern on the supramolecular topological entanglement, PKHB was derivatized with phenylureidohexylcarbamate groups (PU), capable of forming bifurcated H-bonds between the carbonyl acceptor of one urea unit and the two NH donors of another one (Scheme 1). The functionalization conditions are the same as PKHB-ODIN, using phenylureidohexyl isocyanate as reactant (Scheme S3). In the case of PKHB-PU the percentage of functionalization of the phenoxy resin is higher (23% for PKHB-PU vs 13% for PKHB-ODIN). Also in this case, the amount of functionalization is quantified via nitrogen EA (see S1 for complete characterization).

### 3.3 Viscoelastic properties of PKHB-ODIN and PKHB-PU

Viscoelastic properties of PKHB-ODIN and PKHB-PU were studied by means of dynamic mechanical thermal analysis (DMTA). Pristine PKHB exhibits its main relaxation, with  $T_{\alpha}$  at 92 °C, close to its glass transition ( $T_g$ ) measured at 86 °C by differential scanning calorimetry (DSC, Figure S6). The presence of H-bonding moieties causes an increase in the relaxation temperature, dependent on the crosslinking density. Indeed,  $T_{\alpha}$  is shifted to 101 °C for

PKHB-ODIN 8% and 108 °C for PKHB-ODIN 13%, while for PKHB-PU 23% it is further increased to 115 °C (Fig. 4). These temperatures agree with  $T_g$  measured via DSC at 105, 106 and 111 °C for PKHB-ODIN 8%, PKHB-ODIN 13% and PKHB-PU 23%, respectively (Figure S6). For all materials, no stable plateau is observed above the glass transition, as there is no covalent crosslinking. Instead, the storage modulus plots slowly decrease with increasing temperature, reflecting the weakening of H-bonding between polymer chains (Fig. 4). The decay rate of the storage modulus is lower for PKHB-ODIN compared to PKHB-PU and pristine PKHB, reflecting the higher binding energy associated to the sextuple H-bonding.

The viscoelastic properties of PKHB-ODIN were further investigated as described in the SI. Above their glass transition, PKHB-ODIN exhibit fast relaxation kinetics (Figure S7), with limited differences as a function of ODIN %, reflecting the shift in  $T_{\alpha}$ . The response over longer time across the range of the glass transition temperature was studied by creep tests at 100 °C under a low stress (100 kPa) to confirm that higher ODIN grafting decreases the rate of creep relaxation (Figure S8a). Non-isothermal creep tests were also carried out, to evaluate the temperature at which the mechanical relaxation becomes apparent under static conditions (Figure S8b). Under these testing conditions a



**Scheme 1** up functionalization of PKHB with ODIN-isocyanate ( $0.08 < x < 0.13$ ); down functionalization of PKHB with phenylureidohexyl isocyanate ( $x = 0.23$ )

moderate shrinking was observed for both PKHB-ODIN formulations above their glass transitions, reflecting the memory shape effect typical of weakly crosslinked polymer systems. With increasing temperature, the elongation of the specimen under the static load dominates, suggesting that the equilibrium of ODIN dimers is rapidly shifted towards the dissociated form in the temperature range above  $100\text{ }^{\circ}\text{C}$ .

### 3.4 Single Lap Shear (SLS) tests

For this study we selected a CFRP that has valuable mechanical properties in terms of compression strength, but whose interlaminar properties are characterized by not very high values. See Methodology section and SI for details.

Preliminary adhesion tests according to the single lap shear (SLS) configuration were conducted to evaluate the

effect of physical and supramolecular topological entanglement on the adhesion between two plies. In detail, two CFRP panels of  $150 \times 200\text{ mm}$  area were laminated with 8 plies each and the adhesives were deposited on the surface of one plate in a section of  $200 \times 30\text{ mm}$  to cover the overlap length ( $25.4\text{ mm}$  for the used ASTM D5868 standard, see Methodology section for details) to realize single superposition joints. Chemical solution deposition was chosen to apply the adhesive on the ply surface. All pristine phenoxy resins and PKHB-PU are soluble in chloroform. Solubilization of PKHB-ODIN requires the presence of an H-bond acceptor cosolvent to break the sextuple H-bond dimerization cross-linking among polymer chains. We selected hexafluoroisopropanol as cosolvent since it has a boiling point close to that of chloroform ( $58\text{ }^{\circ}\text{C}$  vs.  $61\text{ }^{\circ}\text{C}$ ), so they evaporate almost simultaneously after deposition. Both functionalized

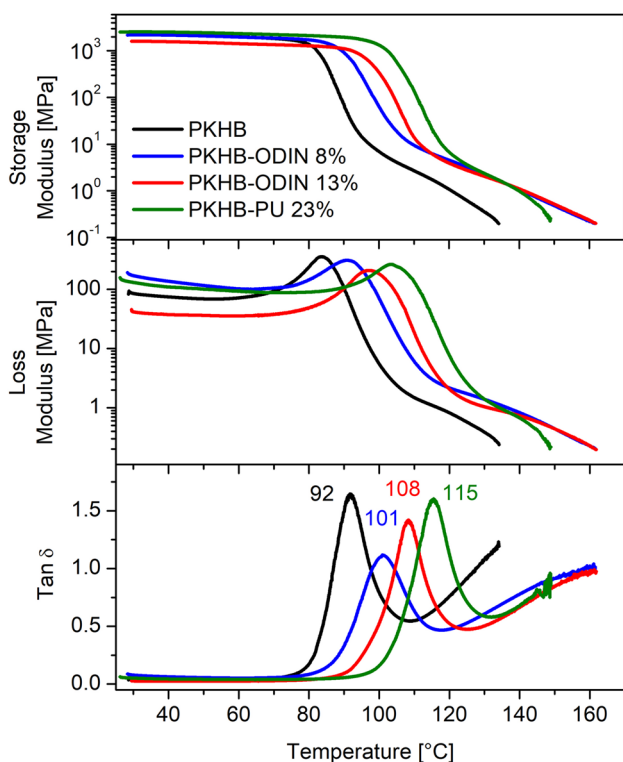


**Fig. 4** DMTA plots (storage modulus, loss modulus and  $\tan\delta$ ) for PKHB and ODIN/PU functionalized counterparts

**Table 1** SLS test results on three different molecular weight phenoxy resin, compared to the pristine standard (average value of 5 specimens for each sample)

	Mw	SLS [MPa]	Standard deviation	Improvement
PKHA	25000	16.6	±1.00	9.2%
PKHB	32000	17.2	±1.00	13.2%
PKHP	52000	14.7	±1.00	-3.4%
Reference	\	15.2	±0.68	\

and non-functionalized resins were dissolved in a 9:1 solution of chloroform and hexafluoro-isopropanol and applied manually by means of a brush on the 30 mm × 200 mm joint area of one of the two prepreg panel plies. The amount of adherent applied in each case is 15% w/w of the total amount of epoxy resin present per area of application. The solvent was left evaporating for one day at room temperature, after which the second panel overlapped in the joint area. The joint panels were placed in a vacuum bag to remove air and subjected to the standard curing cycle in autoclave (90 min, 135 °C, 6 bar) (Fig. 2c). From each panel, six single lap shear specimens were cut and five of them were tested. The adhesion properties of the bonded joints were investigated with single lap shear test configuration, following the ASTM D 5868 – 01 Standard Test Method for Lap Shear Adhesion for Fiber Reinforced Plastic (FRP) Bonding1 standard method. The single lap shear test consists in applying a displacement

**Table 2** SLS test results on PKHB at different levels of ODIN functionalization, compared to the pristine and to the PKHB specimens (average value of 5 specimens for each sample)

	SLS [MPa]	Standard deviation	Improvement (Rif. Reference)	Improvement (Rif. PKHB)
Reference	15.2	±0.68	\	\
PKHB	17.2	±1.00	13.1%	\
PKHB-ODIN 8%	18.5	±1.23	21.7%	7.5%
PKHB-ODIN 13%	18.3	±1.04	20.4%	6.4%
PKHB-PU 23%	14.8	±0.44	-2.6%	-13.9%

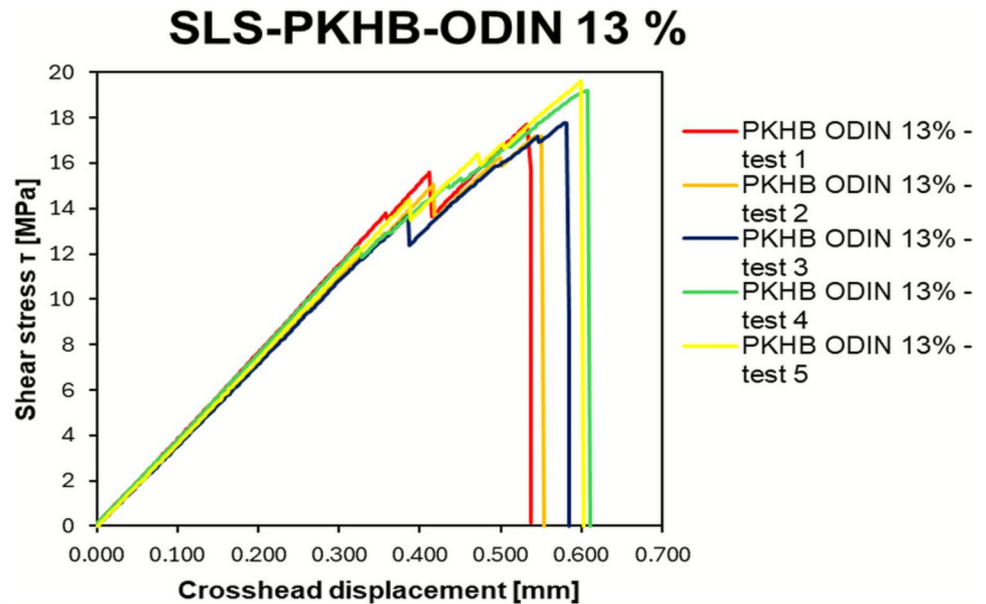
at fixed speed, resulting in increasing stress until the specimen, secured by two clamps, breaks. The shear strength  $\tau$  is obtained by dividing the maximum load by the area of application of the specimen (Figure S9).

The results of SLS test on the three different molecular weight phenoxy resins are summarized in Table 1 (see Figures S10-S12 in SI for the SLS curves) and compared to the reference specimen without added adhesive. All the specimens tested showed a cohesive rupture (shown in Figure S15 for PKHB-ODIN 13%). Both PKHA and PKHB show a substantial improvement in SLS shear strength with respect to the reference, while PKHP produced a small decrease.

The data reported in Table 1 indicates that the Mw of the phenoxy resin significantly affects physical entanglement. Accordingly, PKHB has the appropriate Mw to diffuse into the ply composite matrix. PKHB was therefore selected for ODIN functionalization. Six lap shear specimens were prepared for each grade of ODIN functionalized PKHB (8% and 13%) and for PKHB-PU 23%. Five of them were mechanically tested following the ASTM 5868 standard method and one kept for further analyses.

The results of SLS tests are reported in Table 2 (see Fig. 5 and S13-S14). Figure 5 shows that the five specimens relative to PKHB-ODIN 13%, all tested at room temperature, are characterized by the same stiffness and the damage of the joint area starts around 15 MPa. The specimens show a small delamination (kinks in the curve), regaining the same stiffness until failure, that occurs at around 18–20 MPa. This behavior indicates that the interface, even if it starts to damage, is able to carry the applied load without modifying the overall mechanical properties (the slope of the stress-displacement curve is the same before and after delamination). The linear aspect of the stress-displacement curves indicates a fragile behavior, thus the system under the applied load is not plastically deforming. The presence of ODIN leads to an average 7% increase in SLS with respect to pristine PKHB and to a 21% with respect to reference specimens. By comparison, the control material PKHB-PU 23% exhibits a 13.9% reduction, a clear indication that only multiple H-bonding systems have enough strength to improve SLS in

**Fig. 5** Load—displacement curves for five specimens jointed with PKHB-ODIN 13%



CFRP. The SLS results for PKHB-ODIN 8% and 13% are comparable within the experimental error, indicating that the amount of ODIN in PKHB above 8% does not improve shear strength. We selected PKHB-ODIN 13% as the best candidate for specific delamination tests.

### 3.5 Double Cantilever Beam (DCB) and End Notched Flexure (ENF) delamination tests

There are three different tests to evaluate delamination or interlaminar fracture toughness, based on the direction where the stress is applied to the material. Mode I of delamination is applied when stress is perpendicular to the crack propagation plane, that is tested according to Double Cantilever beam (DCB) configuration, Mode II when stress occurs parallel to this plane, tested according to End Notch Flexure (ENF), and Mode III when out of plane shear is applied (Figure S16). Considering standard composite component loading configurations, Mode I and Mode II fracture toughness tests are the most important to mimic the potential failure of the component due to peeling situations (Mode I) and interlaminar failure (Mode II). For this reason, Mode III loading configuration was not considered in the present study. DCB test is performed following the ASTM D5528-01 protocol (Standard Test Method for Mode I Interlaminar Fracture Toughness of Unidirectional Fiber-Reinforced Polymer Matrix Composites), the ENF test is applied following ASTM D7905/D7905M-19 (Standard Test Method for Determination of the Mode II Interlaminar Fracture Toughness of Unidirectional Fiber-Reinforced Polymer Matrix Composites) procedure (Figures S17-S20). Samples were prepared by laminating two adherends made of 8 plies of CFRP, applying the solution with phenoxy resin

PKNB with and without the specified above functionalizations with the same % in weight of single lap shear configuration. As already explained for single lap shear specimens, the solvent was left evaporating for one day at room temperature, after which the second adherend was overlapped in the joint area. DCB and ENF samples present an initial artificial crack, with initial length  $a_0=25$  mm and  $a_0=55$  mm respectively, that was realized thanks to a polyethylene release film with thickness  $t=0.15$  mm (Figure S17). The joint panels were placed in a vacuum bag to remove air and subjected to the standard curing cycle in autoclave (90 min, 135 °C, 6 bar) (Fig. 2). From each panel, four DCB and four ENF specimens were cut and tested. DCB samples are opened thanks to a specific fixture by applying a constant crosshead of the testing machine that tends to open the joint perpendicularly to the lamination phase. The crack propagation and evolution are measured via digital image correlation (DIC). ENF tests are performed loading the coupons on a three-point bending flexural configuration and observing the crack propagation. Different from what previously explained for DCB, in the case of Mode II testing, once the cracks propagate, a load drop is observed, and the test is concluded. In Mode II cracks propagate in a more sudden and uncontrolled way. Further details about the test realization are reported in the Methodology section. Also, for this test DIC was used to measure crack propagation.

The DCB and ENF procedures were applied to CFRP samples with the following adherends: phenoxy resin PKHB, PKHB-ODIN 13% and PKHB-PU 23%. The histograms of Fig. 6 illustrate the results. All experimental data are reported in Fig. 7, Figures S23-S27 and Table S2 for DCB and Fig. 8, Figures S28-S29 and Table S3 for ENF. Considering the effect of the functionalization on the

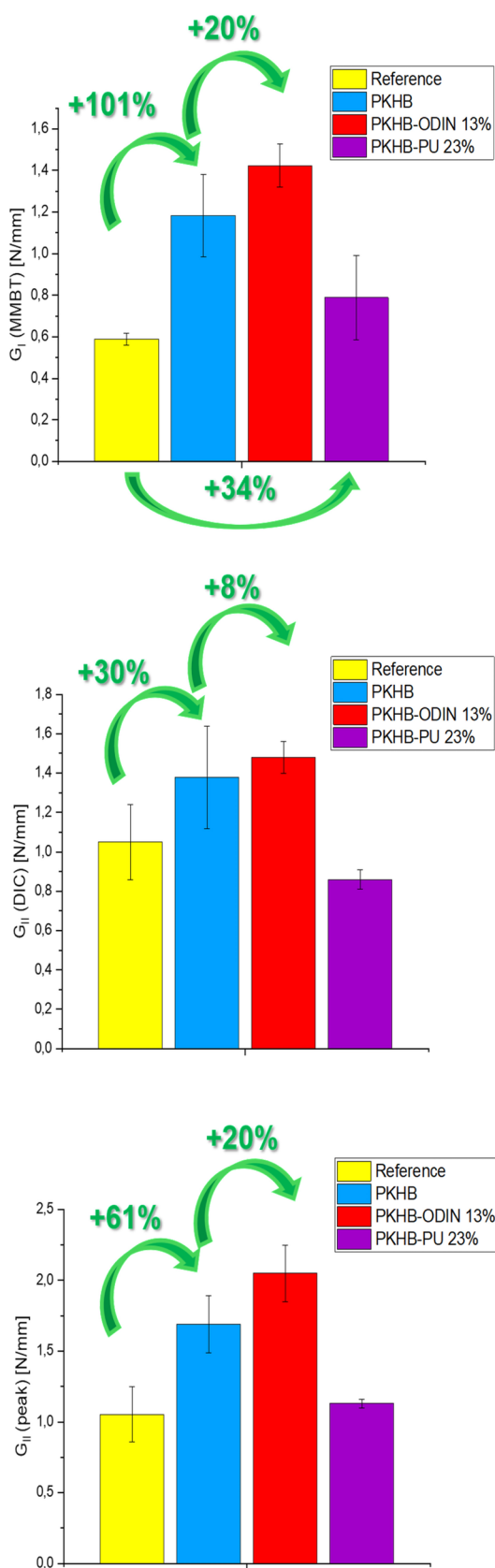


**Fig. 6** **A** DCB  $G_I$  values for the reference material T700 C384 ER450 40% (yellow bar), the medium-molecular weight phenoxy resin PKHB (blue bar), PKHB-ODIN 13% (red bar) and PKHB-PU 23% (purple bar). **B** ENF-DIC  $G_{II}$  values for the reference material, PKHB, PKHB-ODIN 13%, PKHB-PU 23% calculated from the initial point of delamination determined with DIC camera, **C** ENF-PEAK  $G_{II}$  values for the reference material, PKHB, PKHB-ODIN 13%, PKHB-PU 23% calculated from the point of delamination determined with a drop in the load curve determined by the testing machine

**A**

$G_I$  measured values, the addition of PKHB alone results in an increment of  $G_I$  of more than 100% with respect to the reference sample [24, 25], which increases to 120% ( $1.423 \pm 0.185$  N/mm, Table S2) using PKHB-ODIN 13% as adherent. By employing PKHB-PU 23% the  $G_I$  enhancement is reduced to 34% (Fig. 5A). The observed trend can be explained as follows: the physical entanglement by PKHB is able to enhance significantly the energy required to propagate the crack in Mode I configuration and its effect is further amplified by the supramolecular topological entanglement given by ODIN dimerization within the epoxy matrix. The reduced increment observed for PKHB-PU 23% (Fig. 5A) demonstrates that what is important is the strength of topological H-bonding rather than its number. Thus, the ODIN-functionalized phenoxy chains of PKHB connect the interfaces of the chosen CFRP materials realizing a network that reduces crack propagation both via physical entanglement and multiple H-bond cross-linking. As a crack propagates, the polymer chains at the crack front are stretched, transmit stress from the crack front into the bulk, and break the sacrificial ODIN H-bonds.

**B**

The positive effect of both physical and topological entanglement is further confirmed by  $G_{II}$  energy calculated values via ENF test (Fig. 8). The point of delamination in the ENF tests has been determined in two ways: initial displacement measured by the Digital Image Correlation (DIC) camera and the drop in the load curve determined by the electromechanical testing machine. The first set of data is the most conservative, while the second one gives a more realistic picture of the real behavior. Accordingly, the results reported in Fig. 5B and 5C differ significantly, but in both cases the positive trend in delamination resistance is confirmed. In detail, physical entanglement leads to a 30%  $G_{II}$  increase with DIC analysis compared to a 61% increase via load curve drop ( $2.05 \pm 0.20$  N/mm, Table S3). Topological entanglement adds a further 8%  $G_{II}$  improvement with DIC and leads to a remarkable 20% increment via load curve drop. Also in this case, PKHB-PU 23% shows either a negative trend or a reduced increment, confirming the trend already observed in DCB tests.

**C**

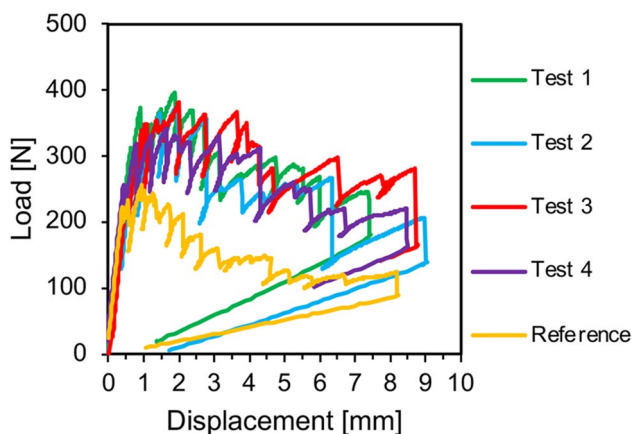


**Fig. 7** Load—displacement curves for PKHB-ODIN 13% specimens (colored lines) compared to average data of 4 reference specimens without any adhesive (yellow line)

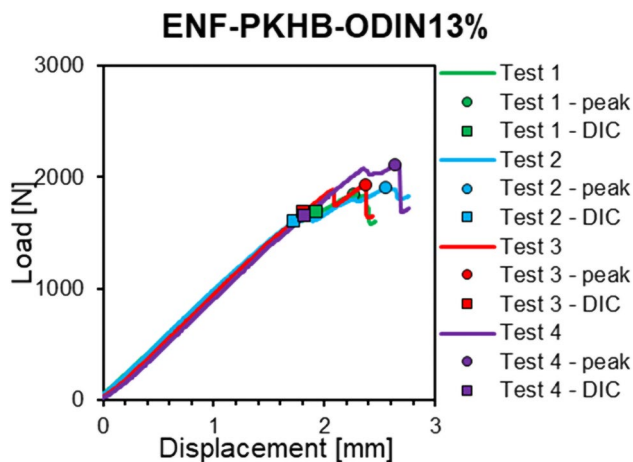


**Fig. 8** Resistance curves for PKHB-ODIN 13% specimens. The colored dots represent the point of crack propagation monitored by the MTS machine, while the colored circles represent the point of delamination determined by the DIC camera

ENF results confirm the behavior observed with DCB tests, however the increments are smaller. The increment is less evident in this configuration because Mode II is a shear loading configuration in which the interfacial layers are expected to move the one with respect to the other, as it is reported in Figure S16. The crack propagation is quite rapid and, in this case, physical and topological entanglements that keep the two interfacial layers together are orthogonal to the shear plane and subjected as well to shear forces. Even if their presence changes the interface state, they are less efficient in postponing the crack development.

As shown by the error bars reported in Fig. 5, dispersion in  $G_I$  and  $G_{II}$  data is not small. This is normal for these types of tests, since the crack propagation is a phenomenon involving several plies interfaces and the calculation of the

$G_I$  and  $G_{II}$  values are affected by several sources of errors that are due to the parameters used (see equations in the SI).

The fracture surface of the propagation region in DCB and ENF specimens was evaluated by SEM. The morphologies of the DCB fracture surfaces of the reference composite compared to PKHB-ODIN 13% modified composite samples are illustrated in Figure S32. The reference material shows brittle failure with intact carbon fibers, while the PKHB-ODIN 13% modified composite exhibits a rougher surface, reflecting an increased fracture path and ductile failure of the matrix. The surface of the latter is mainly characterized by the matrix in which signs of crack propagation can be evidenced. Similar features are observed in the ENF specimens, as shown in Figure S33. In the case of ENF-PKHB-ODIN 13%, the fracture surface shows multidirectional cracks with a less regular configuration since the loading direction is different and the crack propagation more instable.

#### 4 Quantification of the ODIN dimer formation in PKHB-ODIN and in the epoxy matrix

The key issue of assessing the amount of ODIN present in the dimeric form in the CFRP matrix was addressed via UV–Vis measurements (see SI for methodology, Figure S30), given the different signature of the monomer and the dimer both in solution<sup>21</sup> and in polymeric matrices.<sup>20</sup>

The grade of ODIN dimerization in various polymeric matrices was evaluated on the basis of a thin film (thickness around 100–200  $\mu\text{m}$ ) UV–Vis absorption. The ratio between the two peaks at 340 and 360 nm changes with the degree of dimerization: the peaks have the same height when the molecule is only in his monomeric form, while the blue shifted peak is predominant when dimers are present.<sup>21</sup>

The ratio between the two peaks at 340 nm ( $A_1$ ) and 360 nm ( $A_2$ ) changes with the degree of dimerization: in DMSO solution ODIN is 100% monomer and the  $A_2/A_1$  ratio is 1.01. On the other hand, ODIN is 100% dimer in  $\text{CHCl}_3$  with a  $A_2/A_1$  ratio of 0.61.<sup>21</sup> We estimated the monomer % either by using a linear combination of DMSO and  $\text{CHCl}_3$  solution spectra to fit the ODIN spectra in various resins or by using the following formula (3):

$$\%(Monomer) = \frac{\frac{A_2}{A_1} - \frac{A_2^{CHCl_3}}{A_1^{CHCl_3}}}{\frac{A_2^{DMSO}}{A_1^{DMSO}} - \frac{A_2^{CHCl_3}}{A_1^{CHCl_3}}} \times 100 = \frac{A_2 - 0.6}{0.41} \times 100 \quad (3)$$

obtaining the same results. Applying both methods to the spectra reported in Figs. 9 and S31, we calculated that the percentage of ODIN dimer in PKHB-ODIN 13% resin

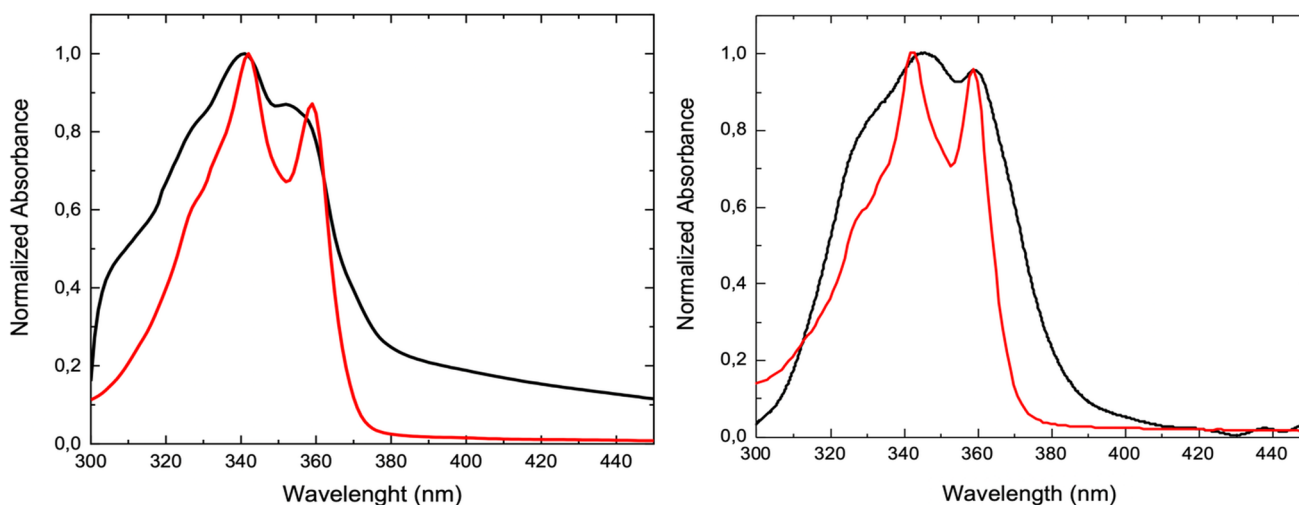


**Fig. 9** Absorption spectrum of solid PKHB-ODIN-13% (black line, left panel) and PKHB-ODIN-13% dispersed (15% w/w) in epoxy-resin (black line, right panel). The red lines are the respective linear combi-

nations of monomer and dimer spectrum used to fit the experimental spectrum and extract the dimer percentage (See SI for more details)

is ~35%, while in the PKHB-ODIN 13% dispersed (15% w/w) in the epoxy resin is ~15%.

We would like to emphasize the novelty and relevance of this analysis to experimentally prove and quantify the presence of H-bonding networks in polymeric matrices. Extension of this methodology to other polymers is ongoing.

## 5 Conclusions

We present a new supramolecular approach to overcome the long-standing issue of low interlaminar adhesion in CFRPs. Supramolecular topological entanglement has proven to be a reliable route to boost interlaminar fracture toughness in CFRP composites via the combination of physical entanglement of PKHB phenoxy resin and topological network of sacrificial ODIN dimers. Two are the major factors responsible for the observed improvement in delamination resistance: (i) the Mw of the phenoxy resin for the physical entanglement, which affects the polymer chain diffusion in the uncured epoxy matrix of the plies; (ii) the amount of ODIN dimer in the cured epoxy matrix, which hinders crack propagation by rising energy dissipation. The two factors have been effectively coupled by functionalizing part of the secondary OHs of the phenoxy resin with ODIN units.

The positive effects of the PKHB-ODIN-13% application are larger for Mode I than Mode II loading configuration: an outstanding increase up to 120% in peeling resistance with respect to pristine material is measured by DCB, while a remarkable 80% improvement in interlaminar resistance is obtained in the ENF-peak mode. This difference can be explained as follows: the physical entanglement that affects

the polymer chain diffusion in the epoxy matrix is much more efficient if the crack propagates perpendicularly to the PKHB chains, thus finding a physical obstacle difficult to overcome. In the case of Mode II configuration, interlaminar properties are enhanced, but once the crack finds a weak point, its propagation suddenly takes place.

Mechanical data and the result interpretation are further reinforced if DSC and DMA data are considered. The presence in PKHB of ODIN and PU dangling chains pushes  $T_g$  of the adhesive toward higher values, helping the interface in responding in a more efficient way to the crack propagation, in analogy with previously reported correlation between  $T_g$  of the adhesive and joint resistance [26]. Considering DMA results, the decay rate of the storage modulus in temperature is lower for PKHB-ODIN compared to PKHB-PU and pristine PKHB, showing that the higher binding energy associated with the sextuple H-bonding is able to slow down the decay of mechanical properties acting as a source of toughening.

The DCB and ENF improvements due to the presence of ODIN roughly match with the ODIN dimer content in the epoxy matrix. Albeit a direct correlation cannot be proven, the presence of sacrificial multiple H-bonding motifs in the polymer matrix exerts a significant role in enhancing delamination resistance in CFRPs. This interpretation is substantiated by the control tests conducted on specimens featuring PKHB-PU 23% as adherent: the observed DCB and ENF results are significantly lower than those of PKHB-ODIN 13%, indicating that the mere presence of H-bonding does not automatically turn into an improvement of interlaminar fracture toughness.

The technological appeal of this innovative solution is very high as it can be used in critical areas where locally

stronger delamination resistance is needed, without affecting the overall behavior of the material or increasing the weight of the final components. For example, this approach can be implemented for critical joints subjected to homologation tests for racing cars components.

**Supplementary Information** The online version contains supplementary material available at <https://doi.org/10.1007/s42114-025-01569-7>.

**Acknowledgements** This work benefited from the equipment and framework of the COMP-HUB Initiative, funded by the Departments of Excellence program of the Italian Ministry for Education, University and Research (MIUR, 2023–2027). Centro Interdipartimentale di Misure “G. Casnati” of the University of Parma is acknowledged for the use of NMR and MS facilities. T. Martinoni and A. Angione are acknowledged for their support in mechanical tests carried out at Dallara Automobili S.p.A. A. Slobodeniuc of Elantas Europe srl is acknowledged for acquiring SEM images.

**Author contribution** M.M.: Investigation, Visualization. S.D.: Investigation. F.B.: Investigation. A.B.: Investigation. A.L.: Methodology, Validation. A.F.: Investigation, Data curation, Methodology. A.P.: Data curation, Resources, Methodology. R.P.: Data curation, Project administration, Writing – review & editing. C.P.: Conceptualization, Supervision, Writing – review & editing. E.D.: Conceptualization, Supervision, Funding acquisition, Writing – review & editing. All authors reviewed the manuscript.

**Funding** Open access funding provided by Università degli Studi di Parma within the CRUI-CARE Agreement. This work was supported by the National Recovery and Resilience Plan (NRRP), Mission 04 Component 2 Investment 1.5 – NextGenerationEU, Call for tender n. 3277 dated 30/12/2021. Project title: Ecosystem for sustainable transition in Emilia-Romagna. Award Number: 0,001,052 dated 23/06/2022, within Spoke1 activities “Materials for sustainability and ecological transition” CUP D93C22000460001. E. D. and A. F. acknowledge the support of PNRR – M4C2 – 11.1 – PRIN 2022 REPRONET (2022TCJRCA). A. L. and A. B. acknowledge the support of IPHOQS “Integrated Infrastructure Initiative in Photonic and Quantum Sciences”, (IR0000016, CUP B53C22001750006). M. M. thanks Dallara Automobili SpA for support of her scholarships.

**Data availability** No datasets were generated or analysed during the current study.

## Declarations

**Conflict of interest** The authors declare no competing interests.

**Open Access** This article is licensed under a Creative Commons Attribution 4.0 International License, which permits use, sharing, adaptation, distribution and reproduction in any medium or format, as long as you give appropriate credit to the original author(s) and the source, provide a link to the Creative Commons licence, and indicate if changes were made. The images or other third party material in this article are included in the article’s Creative Commons licence, unless indicated otherwise in a credit line to the material. If material is not included in the article’s Creative Commons licence and your intended use is not permitted by statutory regulation or exceeds the permitted use, you will need to obtain permission directly from the copyright holder. To view a copy of this licence, visit <http://creativecommons.org/licenses/by/4.0/>.

## References

1. Senol H, Ulus H, Al Nadhari A, Topal S, Yildiz M (2025) Ameliorating tensile and fracture performance of carbon fiber-epoxy composites via atmospheric plasma activation: Insights into damage modes through in-situ acoustic emission inspection. *Composites: Part A* 195:108929. <https://doi.org/10.1016/j.compositesa.2025.108929>
2. Chawla KK, *Composite materials, science and engineering third edition*, ISBN 978–0–387–74364–6, <https://doi.org/10.1007/978-0-387-74365-3> Springer New York
3. Wu X-F, Yarin AL (2013) Recent progress in interfacial toughening and damage self-healing of polymer composites based on electrospun and solution-blown nanofibers: an overview. *J Appl Polym Sci* 130:2225–2237. <https://doi.org/10.1002/app.39282>
4. Sridharan S (2008) *Delamination behaviour of composites*. ISBN 978–1–84569–244–5 Elsevier
5. Bagheri R, Marouf BT, Pearson RA (2016) Toughening of epoxy nanocomposites: nano and hybrid effects. *Polym Rev* 56:70–112. <https://doi.org/10.1080/15583724.2015.1086368>
6. Maccaferri E, Mazzocchetti L, Benelli T, Brugo TM, Zucchelli A, Giorgini L (2022) Self-assembled NBR/Nomex nanofibers as lightweight rubbery nonwovens for hindering delamination in epoxy CFRPs. *ACS Appl Mater Interf* 14:1885–1899. <https://doi.org/10.1021/acsmi.1c17643>
7. Wang Y, Pillai SKR, Che J, Chan-Park MB (2017) High interlaminar shear strength enhancement of carbon fiber/epoxy composite through fiber- and matrix-anchored carbon nanotube networks. *ACS Appl Mater Interf* 9:8960–8966. <https://doi.org/10.1021/acsmi.6b13197>
8. Kaynan O, Hosseini E, Zakertabrzi M, Motta De Castro E, Pérez LM, Jarrahbashi D, Asadi A (2023) Multifunctionality through embedding patterned nanostructures in high-performance composites. *Adv Mater* 35:2300948. <https://doi.org/10.1002/adma.202300948>
9. Sasidharan S, Anand A (2023) Interleaving in composites for high-performance structural applications. *Ind Eng Chem Res* 62:16–39. <https://doi.org/10.1021/acs.iecr.2c03061>
10. Liu W, Sang C, Jin K, Hou J, Yin M (2024) Experimental investigations into damage mechanism in the low-velocity impact and tension-after-impact testing of z-pin reinforced curved CFRP composite. *Polym Compos* 45:5051–5067. <https://doi.org/10.1002/pc.28109>
11. Hong H, Bae KJ, Jung H, Oh Y, You N-H, Lee J-C, Yu J (2022) Preparation and characterization of carbon fiber reinforced plastics (CFRPs) incorporating through-plane-stitched carbon fibers. *Compos Struct* 284:115198. <https://doi.org/10.1016/j.compstruct.2022.115198>
12. Liu J, Xue Y, Dong X, Fan Y, Hao H, Wang X (2023) Review of the surface treatment process for the adhesive matrix of composite materials. *Int J Adhes Adhes* 126:103446. <https://doi.org/10.1016/j.ijadhadh.2023.103446>
13. Al-Furjan MSH, Shan L, Shen X, Zarei MS, Hajmohammad MH, Kolahchi R (2022) Influence of carbon fiber failure mode caused by TiO<sub>2</sub> coating on the high temperature tensile strength of carbon fiber reinforced 7075 Al alloy composites. *JMR&T* 19:2930–2959. <https://doi.org/10.1016/j.jmrt.2023.08.191>
14. Xiong M, Xiong L, Xiong K, Liu F (2023) A new strategy for improvement of interface and mechanical properties of carbon fiber/epoxy composites by grafting graphene oxide onto carbon fiber with hyperbranched polymers via thiol-ene click chemistry. *Polym Compos* 44:5490–5498. <https://doi.org/10.1002/pc.27503>
15. Kostopoulos V, Kotrotsos A, Tatzalis S, Loutas T, Bosman AW (2016) Toughening and healing of continuous fibre

- reinforced composites by supramolecular polymers. *Compos Sci Technol* 128:84–93. <https://doi.org/10.1016/j.compscitech.2016.03.021>
16. Yang J, Bai R, Chen B, Suo Z (2020) Hydrogel adhesion: a supramolecular synergy of chemistry, topology, and mechanics. *Adv Funct Mater* 30:1901693. <https://doi.org/10.1002/adfm.201901693>
  17. Wen YW, Li M, Fan LF, Rong MZ, Zhang MQ (2024) Imparting ultrahigh strength to polymers via a new concept strategy of construction of up to duodecupole hydrogen bonding among macromolecular chains. *Adv Mater* 36:2406574. <https://doi.org/10.1002/adma.202406574>
  18. Soavi G, Portone F, Battezzato D, Paravidino C, Arrigo R, Pedrini A, Pinalli R, Fina A, Dalcanale E (2023) Phenoxy resin-based vinylous urethane covalent adaptable networks. *React Funct Polym* 191:105681. <https://doi.org/10.1016/j.reactfunctpolym.2023.105681>
  19. Tellers J, Canossa S, Pinalli R, Soliman M, Vachon J, Dalcanale E (2018) Dynamic cross-linking of polyethylene via sextuple hydrogen bonding array. *Macromolecules* 51:7680–7691. <https://doi.org/10.1021/acs.macromol.8b01715>
  20. D'Auria S, Pedrini A, Ferraboschi I, Vachon J, Sissa C, Pinalli R, Dalcanale E (2023) Two-photon microscopy as a visual tool for polymer compatibilization monitoring: the PE-EVOH case. *Soft Matter* 19:1900–1906. <https://doi.org/10.1039/D2SM01577C>
  21. Bertocchi F, Marchetti D, Doria S, di Donato M, Sissa C, Gemmi M, Dalcanale E, Pinalli R, Lapini A (2024) Tuning the optical properties through hydrogen bond-assisted H-aggregate formation: the ODIN case. *Chem Eur J* 30:e202302619. <https://doi.org/10.1002/chem.202302619>
  22. Golkaram M, Boetje L, Dong J, Suarez LEA, Fodor C, Maniar D, van Ruymbeke E, Faraji S, Portale G, Loos K (2019) Supramolecular mimic for bottlebrush polymers in bulk. *ACS Omega* 4:16481–16492. <https://doi.org/10.1021/acsomega.9b02126>
  23. Etter MC (1990) Encoding and decoding hydrogen-bond patterns of organic compounds. *Acc Chem Res* 23:120–126. <https://doi.org/10.1021/ar00172a005>
  24. Van Velthem P, Ballout W, Horion J, Janssens YA, Destoop V, Pardoën T, Bailly C (2016) Morphology and fracture properties of toughened highly crosslinked epoxy composites: a comparative study between high and low T<sub>g</sub> tougheners. *Compos-B* 101:14–20. <https://doi.org/10.1016/j.compositesb.2016.06.076>
  25. Van Velthem P, Gabriel S, Pardoën T, Bailly C, Ballout W (2021) Synergy between phenoxy and CSR tougheners on the fracture toughness of highly cross-linked epoxy-based composites. *Polymers* 13:2477. <https://doi.org/10.3390/polym13152477>
  26. Yildrin C, Ulus H, Sas HS, Topal S, Yildiz M (2025) Assessing the fracture and dynamic mechanical performance of CF/PEKK joints bonded with epoxy-based adhesive film for aerospace applications: Impact of thermal and cycling hygrothermal conditions. *Compos-A: Appl Sci Manuf* 190:108659. <https://doi.org/10.1016/j.compositesa.2024.108659>

**Publisher's Note** Springer Nature remains neutral with regard to jurisdictional claims in published maps and institutional affiliations.